



SUPERMASSIVE BLACK HOLE BINARIES AS GALACTIC BLENDERS

HENRY E. KANDRUP

Department of Astronomy, Department of Physics, and Institute for Fundamental Theory, University of Florida, Gainesville, FL 32611

IOANNIS V. SIDERIS

Department of Physics, Northern Illinois University, De Kalb, IL 60115

BALŠA TERZIĆ

Department of Astronomy, University of Florida, Gainesville, FL 32611

and

COURTLANDT L. BOHN

Department of Physics, Northern Illinois University, De Kalb, IL 60115 and Fermilab, Batavia, IL 60510

ABSTRACT

This paper focuses on the dynamical implications of close supermassive black hole binaries both as an example of resonant phase mixing and as a potential explanation of inversions and other anomalous features observed in the luminosity profiles of some elliptical galaxies. The presence of a binary comprised of black holes executing nearly periodic orbits leads to the possibility of a broad resonant coupling between the black holes and various stars in the galaxy. This can result in efficient chaotic phase mixing and, in many cases, systematic increases in the energies of stars and their consequent transport towards larger radii. Allowing for the presence of a supermassive black hole binary with plausible parameter values near the center of a spherical, or nearly spherical, galaxy characterised initially by a Nuker density profile enables one to reproduce in considerable detail the central surface brightness distributions of such galaxies as *NGC 3706*.

Subject headings: galaxies: evolution – galaxies: kinematics and dynamics – galaxies: structure

1. Introduction and Motivation

Understanding the dynamical implications of a supermassive black hole binary near the center of a galaxy is important *both* because of the insights the problem can shed on physical processes associated with a time-dependent potential *and* because, even if it itself is not resolvable observationally, the binary can have directly observable effects.

As is well known to nonlinear dynamicists, a time-dependent potential can induce significant amounts of time-dependent *transient chaos*, an interval during which orbits exhibit an exponentially sensitive dependence on initial conditions, and resonant couplings between the natural frequencies of the time-dependent potential and the frequencies of the chaotic orbits can trigger efficient *resonant phase mixing* (Kandrup, Vass, & Sideris 2003). Like ‘ordinary’ chaotic phase mixing (*e.g.*, Kandrup & Mahon 1994, Merritt & Valuri 1996), this resonant mixing can facilitate a rapid shuffling of orbits on different constant energy hypersurfaces. Even more importantly, however, because the potential is time-dependent the energies of individual orbits are not conserved, so that resonant mixing can also facilitate a shuffling of energies between different constant energy hypersurfaces.

For this reason, resonant phase mixing has important implications for collective relaxation in nearly collisionless systems (Kandrup 2003), *e.g.*, holding forth the prospect of explaining from first principles the striking efficacy of violent relaxation (Lynden-Bell 1967) that has been observed in numerical simulations and inferred from astronomical observations (see, *e.g.*, Bertin 2000). That large scale collective oscillations could trigger very efficient violent relaxation has been shown in the context of one simple model, namely orbits of stars in a Plummer sphere that is subjected to a systematic time-dependence which eventually damps (Kandrup, Vass, & Sideris 2003). The binary black hole problem provides a complementary example of how, via resonant couplings, smaller scale time-dependences can also have a surprisingly large effect.

The binary black hole problem is also interesting because the binary can have directly observable consequences. The fact that energy is not conserved implies the possibility of readjustments in the density profile of stars near the center of a galaxy. In many cases this energy nonconservation means that, on the average, stars near the center gain energy, which im-

plies a systematic transport of luminous matter near the black holes out to larger radii. To the extent, however, that mass traces light, such changes in the density distribution translate into predicted changes in the observed surface brightness distribution because of the presence of such a binary.

In particular, for reasonable choices of black hole masses and orbital parameters, the binary can actually cause an ‘inversion’ in the surface brightness profile, so that surface brightness is no longer a monotonically decreasing function of distance from the center. Indeed, the simplest models which one might envision are adequate to reproduce distinctive features observed in the brightness distributions of such galaxies as NGC 3706, as reported in Lauer *et al* (2002).

The first half of this paper considers the binary black hole problem as an example of how a time-dependent potential can facilitate efficient phase mixing in a galaxy. Section 2 considers the simplest pedagogical example, namely a black hole binary inserted into the (possibly anisotropic) harmonic potential associated with a constant density ellipsoid. Section 3 explores how results from that model are altered by allowing for a more realistic density profile consistent with what has been inferred from high resolution photometry (*e.g.*, Lauer *et al* 1995).

One important issue here involves determining as a function of amplitude (*i.e.*, black hole masses) and frequency (*i.e.*, orbital period) when the time-dependent perturbation can have a significant effect. A second involves determining the degree to which the efficacy of energy and mass transport reflect the degree of chaos exhibited by the orbits, both in the presence and the absence of the perturbation. To what extent, *e.g.*, does efficient energy transport require that a large fraction of the orbits in the time-dependent potential be chaotic? Does resonant phase mixing rely crucially on the presence of transient chaos?

Another issue involves determining the extent to which the bulk manifestations of a black hole binary vary for spherical, axisymmetric, and nonaxisymmetric (*e.g.*, triaxial) galaxies. Is it, *e.g.*, true that spherical and nearly spherical systems are impacted less by the presence of a supermassive binary since, in the absence of the binary, all or almost all of the orbits are regular? In a similar vein, one would like to understand the extent to which the effects of the binary depend on the steepness of the cusp. And, perhaps most importantly, it would seem crucial to determine how the size of the ‘sphere of influence’ of the binary

depends on the size of the black hole orbits and their masses. Perhaps the most important conclusion here is that this ‘sphere’ can be much larger than the size of the black hole orbits. For plausible choices of parameter values, black holes moving along orbits with size $\sim r_h$ can significantly impact the density distribution at radii as large as $\sim 10 - 20r_h$ or more.

All these issues have important implications for determining when a supermassive black hole binary might be expected to have observable consequences. The second half of the paper, Sections 4 and 5, focuses on these consequences. Section 4 considers the genericity of the simple models considered in Section 2 and 3, which assume circular orbits and equal mass black holes, and then focuses on direction-dependent effects which must be understood to determine how potentially observable quantities depend on the relative orientation of the observer and the binary.

Section 5 then focuses in detail on one specific observable prediction, namely that supermassive black hole binaries can alter the density distribution near the center of a galaxy. What this entails is: (i) generating N -body realisations of density distributions consistent with a Nuker Law (Lauer *et al* 1995); (ii) evolving these N -body systems in the fixed time-dependent potential corresponding to the galaxy plus orbiting black holes; (iii) determining how the initial density distribution changes over the course of time; and, (iv) presuming that mass traces light, integrating the resulting density distribution along the line of sight to obtain a surface brightness profile. These are *not* fully self-consistent computations; but they *can* at least provide strong indications as to what the expected effects of the binary would be. The crucial point, then, is that such an exercise results generically in brightness distributions that resemble qualitatively the forms reported in Lauer *et al* (2002); and that by fine-tuning parameters within a reasonable range, one can reproduce many of the details of what is actually observed.

Section 6 summarises the principal conclusions and discusses potential implications.

2. Supermassive Black Hole Binaries in Constant Density Ellipsoids

2.1. Description of the experiments

The computations described here involved orbits evolved in the potential

$$V(x, y, z) = \frac{1}{2} \left(\frac{x^2}{a^2} + \frac{y^2}{b^2} + \frac{z^2}{c^2} \right) - \frac{M}{|\mathbf{r} - \mathbf{r}_1(t)|} - \frac{M}{|\mathbf{r} - \mathbf{r}_2(t)|}, \quad (1)$$

where \mathbf{r}_1 and \mathbf{r}_2 correspond to circular orbits in the $x - y$ plane, *i.e.*,

$$x_1(t) = r_h \sin \omega t, \quad y_1(t) = r_h \cos \omega t, \quad z_1(t) = 0, \quad (2)$$

and $\mathbf{r}_2 = -\mathbf{r}_1$. The axis ratios a , b , and c were all selected to be of order unity, the black hole masses were taken to satisfy $0.005 \leq M \leq 0.05$, and the radius was assumed to be in the range $0.005 \leq r_h \leq 0.5$. (Because the potential corresponds to a constant density ellipsoid, there is an obvious symmetry with respect to the scaling $M \rightarrow kM$ and $r \rightarrow k^{1/3}r$.)

A ‘realistic’ value for the frequency ω can be computed as a function of a , b , c , M , and r_h . Suppose, *e.g.*, that $a = b = c = 1.0$. In this case, if $M \ll M(r_h)$, with $M(r_h)$ the galactic mass contained within radius r_h , the black holes can be viewed as test particles moving in the galactic potential, so that $\omega = 1.0$, independent of r_h . If, alternatively, $M \gg M(r_h)$, the potential associated with the galaxy can be neglected and one is reduced *de facto* to the circular, equal mass two-body problem, for which $\omega = \sqrt{M/4r_h^3}$. However, for the purpose of this Section, ω was viewed as a free parameter so that, for fixed amplitude and geometry, one can explore the response as a function of driving frequency. This enables one to determine the extent to which the response manifests a sensitive dependence on frequency, which can provide important insights into the resonant couplings that generate the response.

The assumptions that the black holes are in circular orbits and that they have equal masses are of course suspect. However, as will be discussed in Section 4, it appears that relaxing these assumptions does *not* change the principal conclusions. *This model appears structurally stable towards modest changes in the orbital parameters of the binary.*

Attention focused primarily on the statistical properties of representative orbit ensembles, integrated

from sets of ≥ 1600 initial conditions. These were generated by uniformly sampling a specified constant energy hypersurface *as defined in the limit* $M \rightarrow 0$ using an algorithm described in Kandrup & Siopis (2003). Allowing for the black holes changes the initial energies, so that one is *de facto* sampling a ‘slightly thickened’ constant energy hypersurface. The initial conditions were integrated forward for a time $t = 512$, with orbital data recorded periodically. The integrations also tracked the evolution of a small initial perturbation, periodically renormalised in the usual fashion (*e.g.*, Lichtenberg & Lieberman 1992), so as to extract estimates of the largest finite time Lyapunov exponent. For a, b , and c of order unity, the dynamical time $t_D \sim 2\pi$, so that $t = 512$ corresponds to an interval $\sim 80t_D$. Sets of simulations were generated by selecting an ensemble of initial conditions, specifying a, b, c, M , and r_h , and then integrating for a number (≥ 100) of different frequencies in the range $0 \leq \omega \leq 24.0$.

For each simulation, specified by a, b, c, M, r_h , and ω , the orbits were analysed to extract the following quantities:

- (i) the fraction f of ‘strongly chaotic’ orbits, estimated as in Kandrup & Siopis (2003) (as discussed in Kandrup, Vass, & Sideris [2003], because the potential is time-dependent it is oftentimes difficult to make an absolute distinction between regular and chaotic orbits, although it *is* relatively easy to identify orbits that are ‘strongly chaotic’);
- (ii) the mean value $\langle \chi \rangle$ of the finite time Lyapunov exponents for the strongly chaotic orbits;
- (iii) the mean value $\langle \delta E \rangle$ of the energy shift $\delta E \equiv E(t) - E(0)$ for all the orbits at various times $t > 0$; and
- (iv) the dispersion $\sigma_{\delta E}$ associated with these shifts.

The data were also analysed to determine the functional forms of $\langle \delta E(t) \rangle$ and $\sigma_{\delta E}(t)$, and to search for correlations between changes in energy and values of finite time Lyapunov exponents for individual orbits within a single ensemble.

In addition to such ‘representative’ ensembles, integrations were performed to track phase mixing in initially localised ensembles, so as to determine the extent to which the observed behaviour resembles ordinary chaotic phase mixing in a time-independent potential (*e.g.*, Merritt & Valluri 1996, Kandrup 1998) or resonant phase mixing in a galaxy subjected to large scale bulk oscillations (Kandrup, Vass, & Sideris 2003).

2.2. Results

2.2.1. Statistical properties of orbit ensembles

Overall, as probed by the shuffling of orbital energies, there is a broad and comparatively efficient resonant response. For fixed values of a, b, c, M , and r_h , the range of ‘interesting’ frequencies ω can be two orders of magnitude or more in breadth. It is evident that *one does not need to ‘fine-tune’ ω to trigger an efficient shuffling of energies.*

Despite this, however, the resonance *can* exhibit substantial structure, especially in spherical systems. In particular, superimposed upon a smooth overall trend, quantities like $\langle \delta E \rangle$ can exhibit a complex, rapidly varying dependence on ω .

Consider, *e.g.*, Fig. 1, the bottom panels of which exhibit $\langle \delta E \rangle$ and $\sigma_{\delta E}$ at time $t = 512$ as functions of ω for two models, one that is spherical with $a^2 = b^2 = c^2 = 1.0$ and the other triaxial with $a^2 = 1.33, b^2 = 1.0$, and $c^2 = 0.80$. Both models have $M = 0.05$ and $r_h = 0.3$. The curves for the two models have envelopes with a comparatively simple shape but, for the spherical model, an enormous amount of substructure is superimposed. This substructure reflects the idealised assumption of a harmonic oscillator, which implies that all unperturbed orbits oscillate with the same frequency. Indeed, a close examination of Figs. 1 (c) and (d) reveals that the resonances are associated with integer and (to a lesser degree) half-integer values of ω , harmonics of the natural frequency $\omega = 1.0$ associated with the unperturbed orbits. Allowing for an axisymmetric system leads to two characteristic frequencies, which can exhibit a yet more complex response pattern. If, however, M and r_h are chosen large enough to elicit a significant response, the resonances typically broaden to the extent that much, if not all, that structure is lost. Allowing for a fully triaxial system leads to three unequal frequencies, which yields a plethora of harmonics that, even for comparatively weak responses, the short scale structure is largely lost.

It is evident from Fig. 1 that, although $\langle \delta E \rangle$ is substantially larger for the triaxial than for the spherical model, $\sigma_{\delta E}$ is comparable. What this means is that, even though the spherical model leads to a smaller systematic shifting in energies, the energies of orbits in these two models are shuffled to a comparable degree. The observed differences in $\langle \delta E \rangle$ do *not* reflect the fact that the nonspherical model is triaxial. Rather, they appear again to reflect the fact that, for

a spherical system, there is only one characteristic frequency for the unperturbed orbits. Modest deviations from spherical symmetry, be these either axisymmetric or not, suffice typically to yield amplitudes more closely resembling Fig. 1 (g) than 1 (c).

For a specified set of initial conditions and a given set of values for a , b , c , and r_h , there appears to be a threshold value of M below which no substantial response is observed; and, similarly, the response ‘turns off’ for higher energy orbits that spend most of their time far from the binary. However, for ‘interesting’ choices of M , as probed, *e.g.*, by $\langle \delta E(\omega) \rangle$ or $\sigma_{\delta E}(\omega)$, the resonance has a characteristic shape. As the frequency increases from $\omega = 0$, $\langle \delta E \rangle$ and $\sigma_{\delta E}$ exhibit a rapid initial increase, peak at a maximum value, and then begin a much slower decrease. For fixed parameter values, *the value of the frequency triggering the largest response is roughly independent of mass*, but it *is* true that, for larger values of M , the relative decrease in $\langle \delta E(\omega) \rangle$ and $\sigma_{\delta E}(\omega)$ with increasing ω is slower than for smaller M . It seems natural to suppose that this reflects the fact that, for larger amplitude perturbations, higher order harmonics become progressively more important. Examples of this behaviour are exhibited in Figs. 2 (a) and (b).

Alternatively, for fixed values of a , b , c , and M , the location of the peak frequency is a decreasing function of r_h . In particular, when the black holes are closer together one requires higher frequencies to elicit a significant response. Examples of this behaviour are illustrated in Figs. 2 (c) and (d).

Efficient shuffling of energies seems tied unambiguously to the presence of large amounts of chaos, as probed by the fraction f of strongly chaotic orbits and, especially, the size of a typical finite Lyapunov exponent. Large f and $\langle \chi \rangle$ do not guarantee large changes in energies, but they are an essential prerequisite. In some cases, notably nearly spherical systems, f and $\langle \chi \rangle$ are very small in the limit $\omega \rightarrow 0$. As ω increases, however, f and especially $\langle \chi \rangle$ also increase; and, for values of ω sufficiently large to trigger an efficient response, the ensemble will be very chaotic overall. For values of ω in the resonant region, f and $\langle \chi \rangle$ tend to exhibit only a comparatively weak dependence on ω . As in Fig. 1 (f), the mean $\langle \chi \rangle$ often exhibits a modest *decrease* at frequencies where the resonance is strongest, but the effect is not all that large. This decrease likely arises because the orbits having acquired higher energies, tend to spend their time at larger radii, further from the binary.

2.2.2. Shuffling of energies as a diffusion process

Overall, the shuffling of energies induced by the black hole binary is diffusive, although the basic picture depends on the amplitude of the response.

When the changes in energy experienced by individual orbits are relatively small, it is the dispersion that tends to grow diffusively, *i.e.*,

$$\sigma_{\delta E} \propto t^{1/2}. \quad (3)$$

In this case, the mean shift in energy typically grows more quickly in time, being reasonably well fit by a linear growth law $\langle \delta E \rangle \propto t$. Alternatively, when the response is stronger, it is the mean shift that grows diffusively, *i.e.*,

$$\langle \delta E \rangle \propto t^{1/2}, \quad (4)$$

whereas the dispersion is well fit by a growth law $\sigma_{\delta E} \propto t^{1/4}$. Examples of both sorts of behaviour can be seen in Fig. 3.

One might naively have supposed that, since the shuffling of energies is associated with the presence of chaos, changes in energy should grow exponentially. This however, does *not* appear to be the case. One cannot exclude the possibility that the initial response of the orbits ($t < 5t_D$ or so) is exponential, but it is evident that, overall, the response is diffusive. *Time-dependent chaos does not trigger exponentially fast mixing in energies. However, it can still be extremely important in that it allows comparatively efficient shufflings of energies that would be completely impossible in a time-independent Hamiltonian system.*

One final point should be stressed. That changes in energy are diffusive, reflecting a slow accumulation of energy shifts, corroborates a fact also evident from an examination of individual orbits: Changes in energy experienced by individual orbits do *not* result from single close encounters with the black holes. Instead, they really do reflect resonance effects associated with the time-dependent potential.

2.2.3. Correlations amongst orbital properties for different orbits within an ensemble

Orbits with smaller finite time Lyapunov exponents χ tend to exhibit energy shifts that are smaller in magnitude $|\delta E|$. Orbits with large χ can experience both large and small net changes in energy, but the energies of orbits with small χ invariably remain nearly constant.

This conclusion holds for both strong and weak responses, but there *is* one important difference: When the response is weak, so that it is the dispersion of the ensemble that evolves diffusively, changes in energy exhibited by individual orbits are comparably likely to be positive or negative. However, when the response is stronger, so that it is the mean shift that evolves diffusively, the energies of individual orbits tend instead to increase systematically.

When the response is relatively weak and changes in energy are equally likely to be either positive or negative, the distribution of energy shifts $n(\delta E)$ is typically well fit by a Gaussian with mean roughly equal to zero. However, when the response becomes stronger, the distribution of energy shifts becomes distinctly asymmetric and cannot be well fit by a Gaussian, even allowing for a nonzero mean.

Correlations between the ‘degree’ of chaos and the ‘degree’ of energy shuffling experienced by individual orbits are perhaps best illustrated by extracting energy shifts δE at different times t_i for *individual orbits*, computing the mean and dispersion, $\langle \delta E \rangle$ and $\sigma_{\delta E}$, associated with the resulting time series $\{\delta E(t_i)\}$, and demonstrating how these moments correlate with the value of the finite time Lyapunov exponent χ . Examples of such an analysis are exhibited in Fig. 4. The obvious point is that the moments are invariably small when χ is small, whereas larger χ typically implies larger values of $|\langle \delta E \rangle|$ and $\sigma_{\delta E}$.

2.2.4. Chaotic and resonant phase mixing

The presence of the supermassive black hole binary will facilitate efficient chaotic phase mixing whenever the orbits have a large finite time Lyapunov exponent. For frequencies ω well out of the resonance region, chaotic orbits behave in much the same fashion as they would in a time-independent potential, and the resulting chaotic phase mixing closely resembles what has been observed in other contexts (*e.g.*, Merritt & Valluri 1996, Kandrup 1998). If, however, ω is in the resonance region, the chaotic phase mixing becomes more complex in that there is also a shuffling of orbits between different constant energy hypersurfaces. This implies that the (necessarily time-dependent) ‘well-mixed’ states observed at later times are statistically different from the (nearly) time-independent state that would arise for $\omega = 0$. In particular, the time-dependence leads generically to changes in such physically observable quantities as the mass density $\rho(\mathbf{r})$.

The behaviour observed for ensembles evolved in the potential (1) is qualitatively similar to that observed for ensembles in the Dehnesque potentials described in Section 3.

3. Supermassive Black Hole Binaries in Cuspy Galaxies

3.1. Description of the experiments

The computations described in this Section involved orbits evolved in a more realistic galactic potential of the form

$$V(x, y, z) = -\frac{1}{(2-\gamma)} \left[1 - \frac{m^{2-\gamma}}{(1+m)^{2-\gamma}} \right] - \frac{M}{|\mathbf{r} - \mathbf{r}_1(t)|} - \frac{M}{|\mathbf{r} - \mathbf{r}_2(t)|}. \quad (5)$$

Here

$$m^2 = (x/a)^2 + (y/b)^2 + (z/c)^2, \quad (6)$$

γ is the cusp index, assumed to satisfy $0 \leq \gamma \leq 2$, and \mathbf{r}_1 and \mathbf{r}_2 are again given by eq. (2).

For $a = b = c = 1$, this potential reduces to the spherical Dehnen (1994) potential with unit mass, and, quite generally, for large r , $V \rightarrow -1/m$. It follows that, for axis ratios of order unity, one can interpret eq. (5) as a potential for a galaxy with mass $M_g \approx 1.0$. For nonspherical systems, eq. (5) yields density distributions different from the triaxial Dehnen models first considered by Merritt & Fridman (1996), in that it is V , rather than ρ , that is constrained to manifest ellipsoidal symmetry.

This potential is unrealistic in that, for large radii, V does not become spherically symmetric; and one can also argue that it is unrealistic in the sense that, assuming mass traces light, the isophotes become peanuty for axis ratios far from spherical. Given, however, that one is interested primarily in physical processes in the central portions of the galaxy, the $r \rightarrow \infty$ asymptotic behaviour is largely unimportant; and it should be recalled that the isophotes in ‘real’ galaxies tend to manifest systematic deviations from ellipticity (*e.g.*, Kormendy & Bender 1996). This potential has the *huge* advantage that, unlike Merritt and Fridman’s nonspherical Dehnen potential, it can be expressed analytically, thus reducing by two orders of magnitude or more the time required for orbital integrations. Moreover, as discussed in Section 5, for the case of spherical symmetry the behaviour of orbits in this potential is very similar to orbits evolved

in the potential associated with a Nuker Law, at least for those choices of Nuker parameters for which the potential can be expressed analytically.

For spherical systems with $a = b = c = 1.0$,

$$M(r) = [r/(1+r)]^{(3-\gamma)} \quad (7)$$

represents the total mass within a distance r of the galactic center. For axis ratios of order unity, eq. (7) also provides a reasonable estimate for moderately nonspherical systems.

As for the computations described in Section 2, the computations here involved axis ratios of order unity, masses in the range $0.005 \leq M \leq 0.05$, and radii satisfying $0.005 \leq r_h \leq 0.5$. Integrations again extended for times $0 < t < 512$. Following Merritt and Fridman's (1996) normalisation for their triaxial Dehnen model, one can translate the dimensionless model into physical units by defining the correspondence

$$t = 1 \quad \Leftrightarrow \quad 1.46 \times 10^6 M_{11}^{-1.2} a_{\text{kpc}}^{3.2} \text{ yr}, \quad (8)$$

where

$$M_{11} = \left(\frac{M}{10^{11} M_{\odot}} \right) \quad \text{and} \quad a_{\text{kpc}} = \left(\frac{a}{1 \text{ kpc}} \right).$$

One can identify an energy-dependent dynamical time t_D following either Merritt and Fridman, who related it to the period of a specific type of regular orbit, or following Kandrup & Siopis (2003), who proposed an alternative prescription based on the times between turning points in representative orbits. Those two prescriptions yield results in agreement at the 5% level or better. More generally, for axis ratios of order unity, at least for small radii the angle-averaged density and energy distributions are relatively similar to those associated with a 'true' maximally triaxial Dehnen model, so that a dynamical time $t_D(E)$ can be estimated to within 20% or so from Table 1 in Merritt & Fridman (1996). This implies, *e.g.*, that, for $\gamma = 1.0$, a time $t = 512$ corresponds to roughly $100t_D$ for stars in the 20% mass shell or, equivalently, $\sim 8 \times 10^8 M_{11}^{-1/2} a_{\text{kpc}}^{3/2}$ yr.

As in the preceding Section, ω was often treated as a free parameter, although particular attention did focus on realistic values. For a spherically symmetric system with black hole masses and radii satisfying $M \ll M(r_h)$,

$$\omega^2 = r_h^{-\gamma} (1+r_h)^{\gamma-3}, \quad (9)$$

so that, *e.g.*, $\omega = r_h^{-1/2} (1+r_h)^{-1}$ for $\gamma = 1.0$. Alternatively, for $M \gg M(r_h)$, once again $\omega = \sqrt{M/4r_h^3}$. For $\gamma = 1.0$, $M = 0.01$, and $r_h = 0.05$, fiducial values considered in many of the computations, the galactic potential can be neglected in a first approximation, so that $\omega \approx \sqrt{20} \approx 4.47$.

3.2. Results

3.2.1. Similarities and differences

Overall, the behaviour of ensembles evolved in the potential (5) is strikingly similar to what was observed for the oscillator potential (1), even for cusp indices $\gamma \neq 0$ and/or orbits with relatively large energy, for which the form of the potential is quite different. This suggests strongly that *the qualitative form of the behaviour observed for the oscillator model is generic*. The only obvious difference between the two models is that the short scale resonance substructure, especially prominent when $a = b = c$, is completely lost. Because the force is no longer linear, different unperturbed orbits, even those with the same energy, have different natural frequencies, so that the resonance is not dominated by a single frequency.

Overall, spherical, axisymmetric, and triaxial systems exhibit broad resonance patterns that are similar in shape one to another *and* to the patterns observed for the oscillator model, although some relatively minor differences *do* exist. Fig. 5 exhibits data for two models, one spherical and the other triaxial, each with $\gamma = 1.0$, $r_h = 0.05$, and $M = 0.01$. The models were both generated for ensembles of initial conditions with $E = -0.70$ and $\langle r_{in} \rangle \approx 0.33$. The black hole radius $r_h = 0.05$ corresponds roughly to the 0.2% mass shell.

These models are representative in the sense that modest changes in the parameters of the binary do not lead to significant qualitative changes in the response. Equally important, however, they are also robust towards changes in axis ratio. Axisymmetric and slightly triaxial models (*e.g.*, as nonspherical as $a^2 = 1.05$, $b^2 = 1.00$, and $c^2 = 0.95$) yield results very similar to the spherical case. 'Strongly' triaxial models yield results similar to the particular triaxial model exhibited here.

Analyses of these and other models lead to the conclusion that, even for systems that are spherical or nearly spherical, the relative measure f of strongly chaotic orbits tends to be large even when $\omega = 0$, this corresponding to two stationary but separated black holes. *One does not require a strong time-*

dependence to generate a large measure of chaotic orbits. What *is*, however, true is that, for axisymmetric and other nearly spherical systems, the degree of chaos, as probed by $\langle\chi\rangle$, tends to be considerably smaller than is the case for strongly triaxial systems.

In significantly triaxial models, the degree of chaos, as probed by f or $\langle\chi\rangle$, is a comparatively flat function of ω . By contrast, in nearly spherical and axisymmetric systems, the degree of chaos, especially as probed by $\langle\chi\rangle$, increases rapidly with increasing ω until it becomes comparable to the degree of chaos exhibited by strongly triaxial models. The obvious inference is that, *when the system is nearly spherical or axisymmetric, the time-dependence associated with the orbiting binary is required to give the chaotic orbits particularly large Lyapunov exponents.*

This has an important practical implication: Although the degree of chaos and the amplitude of the response tend to be comparable at high frequencies for models with very different shapes, at relatively low frequencies nearly axisymmetric models tend to exhibit less chaos and a weaker response. For the black hole parameter values in the models used to generate Fig. 5, a realistic frequency corresponds to $\omega \sim \sqrt{20}$. It is, however, evident that, for such a low frequency, $\langle\chi\rangle$ is substantially smaller for the spherical model than for the triaxial model; and it is even more evident that this is reflected by smaller values of $\langle\delta E\rangle$ and $\sigma_{\delta E}$.

Consider, however, a real supermassive black hole binary which, presumably, starts off at a large distances from the center of a galaxy with significantly eccentric orbits that, as a consequence of dynamical friction (Merritt 2001) slowly decay to smaller, more nearly circular orbits. When the black holes are in relatively large orbits, they will have a comparatively minimal effect on the mass distribution of the galaxy. In part this is because the force that they exert on the ambient stars is typically compared with the force associated with the galaxy as a whole. This, however, is not the whole story. Equally important is the fact that, when the orbit is very large, the orbital frequency ω is very small.

Typically, the black holes only become an important source of energy and mass transport once their orbits have decayed to the point that the black hole masses become comparable to, or larger than, $M(r_h)$, at which point an efficient resonance can be triggered. This, however, does *not* mean that the black holes only have a significant effect at distances $\leq r_h$.

Rather, once the resonance has been triggered, it can impact orbits which, on the average, are much further from the center of the galaxy: the triaxial model in Fig. 5 shows that a binary with $r_h = 0.05$ can induce very large effects on orbits with $\langle r_{in} \rangle > 6r_h$.

The crucial point in all this is that, because larger frequencies are required to trigger the resonance in galaxies that are nearly axisymmetric, *in axisymmetric and other nearly spherical galaxies black holes of given mass must be in a tighter orbit before they can trigger a significant response.* Concrete examples of this will be discussed in Section 4.

3.2.2. Chaotic and resonant phase mixing

The time-dependent potential associated with the black hole binary can alter ‘ordinary’ chaotic phase mixing in at least two important ways.

The time-dependent potential tends to enhance the degree of chaos in the system, increasing both the fraction of chaotic orbits and the size of a typical Lyapunov exponent. To the extent that the bulk potential of a galaxy is in a time-independent equilibrium or near-equilibrium state, the relative measure of (at least strongly) chaotic orbits should be relatively small, since presumably one requires large measures of regular (or nearly regular) orbits to provide the ‘skeleton’ of the interesting structures that are associated with those chaotic orbits which *are* present (Binney 1978). As discussed above, introducing a time-dependent perturbation leads oftentimes to a significant increase in the relative measure of chaotic orbits. Moreover, even when the time-dependent potential does not significantly increase the measure of chaotic orbits, it can make already chaotic orbits more unstable, thus allowing them to mix more efficiently.

Because energy is no longer conserved, the time-dependent potential also facilitates mixing between different constant energy hypersurfaces, which is completely impossible in the absence of a time-dependence. As discussed already, the time-dependent potential does not in general allow energies to change exponentially fast; and it is also evident that, *as probed by their energies, two initially nearby chaotic orbits will not diverge exponentially.* This implies that mixing of energies is not as efficient a process as mixing in configuration or velocity space. However, the resonant mixing of energies associated with chaotic orbits still plays an important role in shuffling the orbits.

An example of such resonant phase mixing is pro-

vided in the left panels of Fig. 6, which track the evolution of an initially localised ensemble with $E = -0.70$ in a spherical Dehnen potential with $\gamma = 1$ and $a = b = c = 1.0$, allowing now for black hole parameters $M = 0.005$, $r_h = 0.05$, and $\omega = \sqrt{10}$. The right panels track the same ensemble, evolved identically except that $\omega = 0$. Two points are immediate. One is that, for the realistic case when $\omega \neq 0$, a time $t = 64$, corresponding to $\sim 10^8 M_{11}^{-1/2} a_{\text{kpc}}^{3/2}$ yr, is sufficient to achieve a comparatively well mixed configuration. Achieving a comparable degree of mixing for the $\omega = 0$ system requires a time $t > 512$. The other point is that orbits in the ensemble evolved with $\omega \neq 0$ have diffused to radii $r > 0.3$, which is impossible for orbits in the $\omega = 0$ ensemble, for which energy is conserved.

4. Observational Consequences of the Dynamics

4.1. Genericity of the idealised model

Attention hitherto has focused on the dynamical consequences of a supermassive black hole binary, viewed as the prototype of a time-dependent perturbation acting in a galaxy idealised otherwise as a collisionless equilibrium. The object of this and the following Section is to consider instead potentially observable consequences, the most obvious of which is a changing surface brightness distribution induced by a readjustment in the mass density as stars are transported to larger distances from the center of the galaxy.

To understand the origins of such observational consequences, one can proceed by viewing the host galaxy as a superposition of orbit ensembles with different energies E and, for different choices of binary parameters, determine when, for any given value of E , the binary can have an appreciable effect, *e.g.*, by generating a large energy shift $\langle \delta E \rangle$. The results described in the preceding Section indicated that the response will only be large when the size r_h of the binary orbit is sufficiently small that the total black hole mass $M_1 + M_2 \geq M(r_h)$. This, however, implies that, in a first approximation, one is justified in assuming that the frequency of the binary can be estimated neglecting the bulk potential of the galaxy, so that, relaxing the assumptions of equal mass black

holes and strictly circular orbits,

$$\omega = \sqrt{\frac{M_1 + M_2}{A^3}}, \quad (10)$$

with A the value of the semi-major axis.

Perhaps the most obvious question here is simply: For fixed E and A , how do quantities like $\langle \delta E \rangle$ depend on the total mass $M_{tot} = M_1 + M_2$? The answer is that, at least for ‘realistic’ binary black hole masses, *i.e.*, M_1 and $M_2 < 0.01 M_{gal}$, $\langle \delta E \rangle$ is a comparatively smooth, monotonically increasing function of M_{tot} . For very small masses, there is essentially no response; but, beyond a critical mass, the precise value of which depends on properties of the host galaxy, the dependence is roughly power law in form, *i.e.*, $\langle \delta E \rangle \propto M_{tot}^p$, with the power p typically in the range $1 < p < 2$. Examples of this behaviour are exhibited in the left panels of Fig. 7, which show the effects of increasing the total mass for five different models, one spherical, one prolate axisymmetric, one oblate axisymmetric, and two genuinely triaxial. This particular set of examples again incorporated circular orbits and equal black hole masses; but, as will be discussed below, these assumptions are not crucial.

A second obvious question is: How small must the binary orbit be in order to elicit a significant response? Physically, one might suppose that the binary was initialised in a comparatively large orbit as the result of a merger of two colliding galaxies; but that the orbit slowly decayed via dynamical friction, allowing the black holes to sink toward the center of the galaxy. However, within the context of such a scenario the crucial issues to determine are (i) when the binary can begin to have a large effect, *i.e.*, how small the orbit must be; and (ii) when the effects of the binary ‘turn off’ again. These issues are addressed in the right panels of Fig. 7, which exhibit $\langle \delta E \rangle$ as a function of r_h for the same five galactic models used to generate the left panels.

Two points would seem evident: (1) The binary has its largest effect when r_h is substantially smaller than the typical radius of the orbits with the specified energy. The ensembles considered here were each comprised of orbits with initial energy $E = -0.70$ and mean radius $\langle r \rangle \approx 0.33$, but the maximum response was observed for a binary with $r_h \sim 0.04$, *i.e.*, a size roughly ten times smaller! This result, perhaps surprising superficially, reflects the fact that mass and energy transport have been triggered by a resonance, rather than by direct binary scatterings of individual

stars with the black holes. One needs a very tight binary orbit to get frequencies sufficiently large to trigger a significant response. (2) As discussed already in Section 3, for the case of the triaxial models, the effects of the binary appear to ‘turn on’ at substantially larger values of r_h than for the spherical and axisymmetric systems. This would suggest that a black hole binary could have an especially large effect in a strongly triaxial galaxy: since the range of black hole sizes that can have an appreciable effect is substantially larger, the time during which the resonance will act should presumably be longer.

But how generic are the idealised computations described in Section 3? It might not seem unreasonable to assume that the black holes follow nearly circular orbits, since dynamical friction will tend to circularise initially eccentric orbits; but the assumption of equal mass black holes is clearly suspect.

Computations show that varying the eccentricity within reasonable bounds has only a comparatively minimal effect. Increasing the eccentricity e from values near zero to a value as large as $e = 0.5$ will not change quantities like $\langle \delta E \rangle$ by more than 25%; and, in general the effect is much smaller even than this. This is, *e.g.*, evident from the left panels of Fig. 8, which were generated for the same five models considered in Fig. 7.

As is evident from the right hand panels of Fig. 8, there is a substantially stronger, systematic dependence on the mass ratio M_2/M_1 . For fixed $M_{tot} = M_1 + M_2$, the largest effects arise for $M_1 \approx M_2$; but even here the dependence on the mass ratio is not all that sensitive. In particular, for all but the triaxial models, the response is a relatively flat function of M_2/M_{tot} for $M_2/M_{tot} > 0.25$ or so, which means that, for fixed $M_1 + M_2$, mass ratios $1/3 \leq M_2/M_1 \leq 1$ yield comparable results. It *is* true that, for fixed semi-major axis A and total mass M_{tot} , the effect of the binary is significantly reduced for $M_2 \ll M_1$, but the reason for this is easily understood: When $M_2 \ll M_1$, the more massive black hole is located very near the center of the galaxy. This implies, however, that, even if the binary has a very high frequency, the more massive black hole remains too close to the center to have an appreciable effect on stars at large radii. The smaller black hole is typically found at much larger values of r , but its mass is too small to significantly impact the surrounding stars.

4.2. Systematic changes in density

Changes in energy induced by transient chaos lead generically to a readjustment in bulk properties like density; and, to the extent that there is an average increase in energy, this readjustment implies a systematic displacement of stars to larger radii. To see how this effect can proceed, one can sample a constant energy hypersurface to generate a set of initial conditions, integrate those initial conditions into the future, and then compare angle-averaged radial density distributions $\rho(r)$ generated at various times $t \geq 0$.

The left panels of Fig. 9 summarise results for a triaxial model with $a^2 = 1.25$, $b^2 = 1.0$, and $c^2 = 0.75$, assuming circular orbits with $M_1 = M_2 = 0.01$, $r_h = 0.05$, and $\omega = \sqrt{20}$. The ensemble of 4800 orbits was constructed such that $E = -0.70$ and $\langle r_{in} \rangle \approx 0.33$. The five panels exhibit the density distributions at $t = 0, 16, 32, 64$, and 128 , the last corresponding physically to a time $\sim 2 \times 10^8 M_{11}^{-1/2} a_{\text{kpc}}^{3/2}$ yr. The right panels exhibit analogous data for the same ensemble and potential but with the black holes held fixed in space, *i.e.*, $\omega \equiv 0$.

As one would expect, the density distribution remains essentially unchanged for the time-independent potential with $\omega = 0$, but the realistic case with $\omega = \sqrt{20}$ leads to a significant readjustment in density. (Minor changes in the $\omega = 0$ model reflect a modest readjustment to the insertion of the fixed binary in an equilibrium generated without a binary.) Already by $t = 16$, a time corresponding to an interval $\sim 2.5 \times 10^7 M_{11}^{-1/2} a_{\text{kpc}}^{3/2}$ yr, there is a pronounced decrease in density in the range $0.3 \leq r \leq 0.5$ and an increase in density at larger radii. Initially the trajectories are restricted energetically to radii $r \leq 0.6$. By $t = 128$, more than 13% of the trajectories are located at radii $r > 1.0$.

4.3. The size of the ‘sphere of influence’

Figure 9 demonstrates that a black hole binary can significantly impact orbits which spend most of their times at radii $\gg r_h$. The obvious question, however, is: how much larger? To answer this question one can evolve collections of ensembles with a variety of different initial radii, and determine how their response varies as a function of r . The results of two such investigations are summarised in Fig. 10. In each case, the configuration corresponded to a spherical Dehnen model with $a = b = c = 1.0$ and a supermassive black hole binary with $M = 0.005$, $r_h = 0.25$, and fre-

quency $\omega = 0.2828$. The left panels are for a model with $\gamma = 0.0$; the right panels for $\gamma = 1.0$.

It is evident that the binary can have a significant effect on orbits even at very large radii. The ‘sphere of influence’ extends out to $r \geq 4$, even though $r_h = 0.25$. It is also apparent that the ensembles which experience the most shuffling in energies, as probed by $\langle |\delta E| \rangle$ and $\sigma_{\delta E}$, are precisely those ensembles with the largest Lyapunov exponent $\langle \chi \rangle$. Indeed, for the $\gamma = 0.0$ and $\gamma = 1.0$ models, the rank correlation between the mean shift $\langle |\delta E| \rangle$ and the mean exponent $\langle \chi \rangle$ for different ensembles, are, respectively, $\mathcal{R}(\langle \delta E \rangle, \langle \chi \rangle) = 0.615$ and 0.613 .

It is also evident that the value of the cusp index γ has a significant effect on the details of the response. The value of γ does *not* have a large effect on the size of the binary ‘sphere of influence’, but it *does* impact the amplitude of the response and how that response correlates with radius. In both cases, there is a significant response for $0.15 \leq r \leq 6.0$, but the response in this range, as probed both by the degree of shuffling in energies, is somewhat larger for the cuspy model. Even more strikingly, however, the presence of the cusp appears to reduce both the size of the Lyapunov exponents and the degree of shuffling at very small radii. For the cusp model with $\gamma = 1.0$, comparatively little shuffling of energies and comparatively small amounts of chaos are observed at radii $\ll r_h$. In the cuspy model, the very lowest energy stars tend to be more regular and to be less susceptible to resonant mixing.

4.4. Anisotropy

To what extent does the mass transport induced by a supermassive black hole binary depend on direction? Even if, *e.g.*, the host galaxy is modeled as exactly spherical, the binary breaks the symmetry and, as such, could introduce anisotropies into a completely isotropic ensemble of stars. This is important since such anisotropies would imply that changes in visual appearance induced by the binary could depend appreciably on the observer’s viewing angle.

As a simple example, one can consider the direction-dependent density distributions associated with a uniform sampling of a constant energy hypersurface which, assuming a spherical potential, implies a spherically symmetric density distribution and an isotropic distribution of velocities. One example thereof is exhibited in Fig. 11, which was generated for

a Dehnen model with $a = b = c = 1$ and $\gamma = 1.0$, containing a binary executing a circular orbit in the $x - y$ plane with the ‘correct’ Kepler frequency. Here the top left panel exhibits spatial distributions at times $t = 0$ and $t = 512$; the top right panel shows the corresponding velocity distributions. At time $t = 0$, the spatial and velocity distributions are all equal modulo statistical uncertainties; at late times they differ systematically, but it remains true that $n(|x|) = n(|y|)$ and $n(|v_x|) = n(|v_y|)$. It is obvious from the left panel that there is a systematic outward transport of stars in all three directions, but it is also evident that, as might have been anticipated, there is a larger net effect on the spatial components in the plane of the orbit. Similarly, there is a modest shift in velocities which, again, is more pronounced in the x and y components. The bottom two panels contain plots of, respectively, the x and y and the x and z coordinates at $t = 512$. Examination of these panels confirm the fact that the initially spherical distribution is more extended in the plane of the binary than in the orthogonal direction. In particular, the resulting density distribution could easily be misinterpreted as a disc or a torus.

But what happens if the host galaxy is already non-spherical? If, *e.g.*, the galaxy is genuinely triaxial, one might perhaps suppose that the binary will have settled into one of the symmetry planes; but, assuming that this is really the case, there are at least two obvious questions that need to be addressed. (1) How does the overall response depend on which symmetry plane? If, *e.g.*, the binary is oriented perpendicular to the long axis, will its net influence be significantly different from its influence if oriented perpendicular to the short axis? (2) For a binary oriented in a given plane, to what extent do observable properties depend on viewing angles?

Both these questions were addressed as before by evolving uniform samplings of constant energy hypersurfaces which yield a triaxial number density but are still characterised by an isotropic distribution of velocities. One example of such a computation is summarised in Fig. 12. Here panel (a) exhibits the density distributions $n(|r_i|)$ at $t = 0$; the remaining three panels exhibit the corresponding distributions at $t = 512$ for three different integrations, with the binary oriented in the $x - y$, $y - z$, and $z - x$ planes.

Overall the ‘angle-averaged’ properties of the different simulations are very similar: The mean short time Lyapunov exponents $\langle \chi \rangle$ for the three different

runs agree to within 10%, and even smaller variations were observed for quantities like $\langle \delta E \rangle$. Indeed, the shape of the galaxy seems more important than the orientation of the binary. For all three binary orientations, one observes that the largest effect is in the x -direction, which corresponding to the long axis, and the smallest in the short-axis z -direction. The details of the response observed here depend to a considerable extent on both the shape of the potential and the energy of the initial ensemble. In particular, for some choices the response is largest in the short-axis rather than long-axis direction. However, it seems true quite generally that the orientation of the binary is comparatively unimportant. There remains a dependence on viewing angle but, if anything, this effect is somewhat weaker than for the case of spherical systems.

For the case of an axisymmetric system with the binary oriented in the $x - y$ symmetry plane, one finds generically that distributions in the x and y directions agree to within statistical uncertainties, but that the z -direction distributions differ systematically. In some cases (depending on both shape and binary parameters), there is more mass transport in the z directions; in others the effect is more pronounced in the x and y directions. These differences likely reflect the fact that this mass transport is triggered by a resonance. The unperturbed orbits have different characteristic frequencies in different directions, but this would suggest that the resonant coupling could well be stronger (or weaker) in one direction than in another.

5. Modeling Luminosity Profiles in Real Galaxies

5.1. Basic strategy

The objective here is to show that the physical effects discussed above, which appear the inevitable consequence of the presence of a supermassive black hole binary in the center of a galaxy, could provide a natural explanation of the fact that, in a number of galaxies that have been observed using *WFPC 2* (e.g., Lauer et al 2002), the projected surface brightness distribution in a given direction is not a monotonically decreasing function of distance from the center of the galaxy.

The computations described here are not completely realistic. As in Section 3, they assume a pair of black holes of exactly equal mass executing exactly circular orbits; and, as in the preceding, the computed

orbits of test stars are not fully self-consistent since one is neglecting both changes in the form of the bulk potential that will arise as stars are displaced from their original trajectories and the fact that the binary orbit slowly decays. They *do*, however, demonstrate that allowing for a binary of relatively small size, ~ 10 pc, comprised of black holes with mass $\leq 1\%$ the mass of the galaxy, leads generically to luminosity dips of the form that have been observed. Moreover, fine-tuning parameters within a reasonable range of values allows for the possibility of a comparatively detailed (albeit in general nonunique) fit to observations of specific galaxies.

The basic programme is as follows:

- Generate N -body realisations of a spherical galaxy characterised by an isotropic distribution of velocities and a Nuker (Lauer *et al* 1995) density profile $\rho(r)$ with specified parameter values.
- Insert into that system a black hole binary with specified masses $M_1 = M_2 = M$ and radius r_h . For ‘realistic’ values of M and r_h , $M(r_h)$ is typically small compared with the black hole mass, so that one can assume, at least approximately, that the black holes are executing a Keplerian orbit with frequency $\omega = \sqrt{M/4r_h^3}$.
- Next evolve the initial conditions in the *fixed* time-dependent potential comprised of the Nuker potential plus the potential of the orbiting black hole binary, and track the radial density distribution $\rho(r)$ as a function of time.
- Finally, assuming that mass traces light, compute line-of-sight integrals along the density distribution to obtain integrated surface densities and, hence, surface brightness distributions as functions of time.

Although this approach does not pretend to be completely realistic, it would not seem totally unreasonable to insert the binary ‘by hand’ without allowing for the dynamics whereby it has evolved into a tightly bound orbit near the galactic center. When the size of the binary orbit is very large, it will have a comparatively minimal effect. Energy and mass transport only becomes important at comparatively small radii, where $M \geq M(r_h)$, and again become unimportant when the radius becomes too small. Most of the action happens for a limited range of radii.

Note, moreover, that the assumption $M \geq M(r_h)$ tends to mitigate the fact that the computations are not fully self-consistent: Although the bulk forces

associated with the galaxy cannot be neglected at all radii where the binary has an appreciable effect, they *can* presumably be neglected, at least approximately, at the comparatively small radii near the binary where the effect of the black holes is strongest.

5.2. The initial form of the density and potential

Initial attempts at modeling using a spherical Dehnen potential yielded results that were in qualitative agreement with observations. However, comparatively large systematic deviations *were* observed, which appeared to reflect the fact that the transition between the inner and outer power-law profiles predicted by a Dehnen potential is too gradual to represent real galaxies. For this reason, models were constructed instead using an initial density distribution satisfying the more general Nuker Law (Lauer et al 1995)

$$\rho_0(r) = \rho_c r^{-\gamma} (1 + r^\alpha)^{\frac{(\gamma-\beta)}{\alpha}}. \quad (11)$$

Dehnen models are recovered for $\alpha = 1$ and $\beta = 4$. The central density ρ_c was chosen so that the total galactic mass $M_g = 1.0$. The associated potential $V(r)$ satisfies (in units with $G = 1$)

$$V(r) = -4\pi \left[\frac{1}{r} \int_0^r \rho(\tilde{r}) \tilde{r}^2 d\tilde{r} + \int_r^\infty \rho(\tilde{r}) \tilde{r} d\tilde{r} \right]. \quad (12)$$

Unfortunately, this potential can be expressed in terms of elementary functions only for certain choices of α and β , which means that, generically, orbits must be computed using an expensive interpolation scheme. This motivated an effort to seek fits assuming values of α and β for which V *can* be expressed analytically. For the small number of profiles considered hitherto, reasonable fits were achieved for $\alpha = 2$ and $\beta = 4$, which, for $\gamma = 0$, corresponds to a potential

$$V(r) = -\frac{2 \tan^{-1} r}{\pi r} \quad (13)$$

and

$$M(r) = \frac{2}{\pi} \left(\tan^{-1} r - \frac{r}{1+r^2} \right). \quad (14)$$

Most models were constructed assuming $M(r_h) \ll M_1 + M_2$, so that the approximation of a Keplerian frequency is typically very good. However, in an effort to allow for the influence of the galactic potential, the models allowed for a slightly modified frequency $\omega = \sqrt{\mathcal{M}/(2r_h)^3}$, where $\mathcal{M} = M_1 + M_2 + 4M(r_h)$.

5.3. Generating a surface brightness distribution

Configuration space was divided into $N = 100$ equally spaced concentric shells i . Each shell corresponded to a range of energies, $E_{i-1} < E < E_i$, $i = 1, \dots, N$, sampled along the principal axes in the plane of the binary, but perpendicular to the line connecting them. This was done to ensure that energy was a monotonic function of radius, so that shuffling of energies could be related directly to a redistribution of orbits in configuration space. Each shell was sampled to select $M = 300$ initial conditions, which were then integrated into the future for a time $t = 512$. Orbital data were recorded at intervals $\Delta t = 128$ and the value of energy at that time was used to reassign the orbit to a (in general) new shell. If $M_i(t)$ denotes the number of orbits in shell i at time t , then

$$\Delta_i(t) = \frac{M_i(t)}{M}, \quad (15)$$

the relative fluctuation in number, can be interpreted as a discretised version of a radial density fluctuation $\delta(t)$ satisfying

$$\rho(r, t) = [1 + \delta(r, t)] \rho_0(r), \quad (16)$$

with ρ_0 the initial density distribution. The smooth $\delta(t)$ was interpolated from $\Delta_i(t)$ using a smooth-curve fitting routine.

The resulting density $\rho(r, t)$ was then integrated along the line of sight to generate a surface brightness

$$\mu(r, t) = \frac{2}{\Upsilon} \int_r^\infty \frac{\rho(\tilde{r}, t) \tilde{r}}{\sqrt{\tilde{r}^2 - r^2}} d\tilde{r}. \quad (17)$$

Here Υ denotes the mass-to-light ratio, which was assumed constant for the modeling described here.

5.4. Results

Figure 13 exhibits data for a typical model, corresponding to a Nuker Law with $\alpha = 2$, $\beta = 4$, and $\gamma = 0$. The binary is comprised of two black holes with $M = 0.005$ and $r_h = 0.15$, yielding a Kepler frequency $\omega = 0.6086$. The half-mass radius of the model is $r = 2.264$, and over 75% of the mass is contained with $r = 5$.

Several points are evident: Most obvious, perhaps, is simply the fact that the binary induces a distinctive signature, characterised by an inversion in both the mass density and the surface brightness profile.

In some cases, especially when $\gamma \neq 0$, the contents of the innermost shells can remain essentially intact. Aside, however, from those innermost shells, one can identify a well-defined sphere of influence in which the binary has observable effects. For $r < r_1$, one observes a systematic underpopulation of stars and, hence, a dip in luminosity; for $r_1 < r < r_2$, one observes a systematic overpopulation resulting from stars that were transported outward from radii $r < r_2$. For $r > r_2$ the density and surface brightness distribution remain essentially unchanged. Also interesting is the fact that the signature, once established, remains unchanged in bulk properties. In particular the dip is comparably prominent visually at $t = 128$ and $t = 512$.

Figure 14 exhibits the result of a more systematic attempt to model the surface brightness of *NGC 3706*, again starting from a Nuker Law with $\alpha = 2$, $\beta = 4$, and $\gamma = 0$. Physical distance was translated into angular separation assuming a scale factor of 0.15, so that, *e.g.*, $r = 1$ corresponds to 0.15 arcsec or, assuming the distance estimate given by Lauer *et al.*, $r \approx 24$ pc. It was again assumed that $M = 0.005$, but, in this case, $r_h = 0.025$, which corresponds to a physical $r_h \sim 0.6$ pc and an angular separation ~ 0.004 arcsec.

It is easy to identify qualitatively three distinct parts of the surface brightness, namely a ‘dip’, a ‘bulge’, and an outermost unperturbed region. The inner dip, extending out to ~ 0.10 arcsec, is a region from which stars have been ejected systematically, so that the surface brightness is lower than what is predicted by an unperturbed Dehnen model. The bulge, which extends out to ~ 0.30 arcsec, corresponding to the region to which those stars have been ejected, is characterised by a surface brightness that is larger than for the unperturbed model. On scales > 0.30 arcsec or so, the binary has only a comparatively minimal effect, so that the surface brightness remains essentially unchanged.

As is evident from the right panels of Fig. 14, the perturbed Nuker model is quite successful in modeling the dip and the outer region, where errors in surface brightness correspond typically to $\delta\mu \sim 0.005$ magnitudes or less. In particular, it is evident that the dip is much better fit by the perturbed model than by an unperturbed Nuker model. Both qualitatively – in the sense that an unperturbed Nuker model requires a monotonically decreasing surface brightness – and quantitatively – in terms of the actual error $\delta\mu$ –, the perturbed model does a much better job. However, both the perturbed and unperturbed mod-

els are somewhat less successful in accounting for the detailed shape of the bulge (although the model with a binary does somewhat better).

There are at least two possible explanations for this lack of success. Most obvious is the fact that, by demanding $\alpha = 2$ and $\beta = 4$, so that the potential could be written in terms of elementary functions, one has limited one’s flexibility in modeling the transition region between the inner and outer (unperturbed) power law profiles. Allowing for fractional values of these parameters (which requires that the potential be computed numerically) will likely yield better fits. However, it is also possible that this lack of success reflects in part the oversimplistic character of the model. In a real galaxy, the binary will slowly drift inwards as a consequence of dynamical friction; and the fact that r_h was not really constant might be expected to have some observable effects. Attempts to remedy these deficiencies of the model are currently underway.

It should, however, be stressed that the general effects computed for the binary are relatively insensitive to r_h , provided only that $M > M(r_h)$. This is, *e.g.*, evident from Fig. 15, the two panels of which exhibit surface brightness distributions at $t = 256$ for both the model considered in Fig. 14 and another model identical except that $r_h = 0.085$. Careful examination reveals some differences in detail, but neither fit is clearly superior visually. It is also evident from Fig. 14 that the basic observable structure develops very quickly. Although the details of the surface brightness profile can vary considerably for times as long $t \sim 128$ or more, the existence of the dip region is obvious already by $t = 32$.

One final point should be noted. Arguing that this sort of dip in surface brightness could be attributed to a supermassive black hole binary does not necessarily imply that the binary is still present. To the extent that, neglecting the binary, the galaxy may be idealised as a collisionless equilibrium, one might expect that a dip in surface brightness, once generated, could persist even after the binary has coalesced, at least for times short compared with the time scale on which stars at larger radii could be scattered inwards via collisional relaxation. To the extent that the bulk potential is time-independent, in the absence of ‘collisions’ energy is conserved, so that an underpopulated region in energy space cannot be repopulated.

6. Discussion

The computations described in this paper yield several potentially significant conclusions regarding phase mixing triggered by a time-dependent potential. Most obvious is the fact that an orbiting supermassive black hole binary can serve as an important source of transient chaos which facilitates efficient resonant phase mixing, shuffling the energies of stars (or any other objects) as well as phase space coordinates on a constant energy hypersurface. In particular, the effects observed here from a comparatively ‘small scale’ perturbation are quite similar qualitatively to the effects observed when galaxies are subjected to larger scale systematic oscillations (Kandrup, Vass, & Sideris 2003). Especially striking, perhaps, is the fact that even though the perturbation is relatively low amplitude and concentrated very near the center of the galaxy, it can have significant effects at comparatively large radii. All this would appear to reinforce the expectation that resonant phase mixing could be a generic physical effect associated with galaxies that are subjected to some oscillatory time dependence.

Contrary, perhaps, to naive expectation, it appears that the shuffling of energies is diffusive, rather than exponential, so that energy phase mixing is less dramatic than phase mixing of coordinates and velocities. Even though the time-dependent perturbation can increase both the relative abundance of chaotic orbits and the degree of exponential sensitivity exhibited by chaotic orbits, it does *not* in general tend to make orbits exponentially unstable in the phase space direction orthogonal to the constant energy hypersurfaces.

However, energy shuffling induced by such transient chaos could still play an important role in explaining violent relaxation. Indeed, the fact that this energy shuffling is not exponential would seem consistent with full self-consistent simulations of violent relaxation (*e.g.*, Quinn & Zurek 1988) which indicate that, even though ‘particles’ in N -body simulations are almost completely ‘randomised’ in terms of most phase space coordinates, they tend to exhibit at least a partial remembrance of initial conditions. In particular, ‘particles’ that start with low (high) binding energies tend systematically to end with low (high) binding energies. If, *e.g.*, stars in simulations involving hard, head-on collisions of galaxies are ordered in terms of their initial and final binding energies, the rank correlation \mathcal{R} between the initial and final

ordered lists typically satisfies (Kandrup, Mahon, & Smith 1993) $\mathcal{R} \geq 0.6$.

That a supermassive black hole binary will cause a systematic readjustment in the density distribution of the host galaxy seems largely independent of the form of the galactic potential or the orbital parameters of the binary, although the precise form of the readjustment does depend on these details. In particular, one sees qualitatively similar effects for Dehnen potentials with different cusp indices γ , and for Nuker Laws with different transitional radii properties. Similarly, the eccentricity and the orientation of the supermassive binary are not crucial, and allowing for unequal, but still comparable, masses does not result in qualitative changes. Irrespective of all these details, one finds that, when the total binary mass $M_1 + M_2 \ll M(r_h)$, with r_h the ‘size’ of the binary orbit, stars cannot resonate with the binary and comparatively little mass transport occurs. However, when $M_1 + M_2 \sim M(r_h)$, one starts seeing substantial effects, effects which can extend to radii $\gg r_h$.

One might therefore expect that (i) when the size of its orbit is large, the binary will have only a minimal effect on the bulk properties of the galaxy; but that when, as a result of dynamical friction (*e.g.*, Merritt 2001), the orbit has decayed to a sufficiently small size, it will begin to have an appreciable – and observable – effect.

HEK acknowledges useful discussions with Christos Siopis, who tried to convince him of the importance of explaining luminosity ‘dips’ months before he was ready to listen. HEK, IVS, and BT were supported in part by NSF AST-0070809. IVS and CLB were supported in part by Department of Education grant G1A62056. We would like to thank the Florida State University School of Computational Science and Information Technology for granting access to their supercomputer facilities.

REFERENCES

- Bertin, G. 2000, *Dynamics of Galaxies*, Cambridge University Press, Cambridge
- Binney, J. 1978, *Comments Astrophys.*, 8, 27
- Dehnen, W. 1993, *MNRAS*, 265, 250
- Kandrup, H. E., 1998, *MNRAS*, 301, 960
- Kandrup, H. E., 2003, in: *Springer Lecture Notes in Physics*, in press (astro-ph/0212031)
- Kandrup, H. E., Mahon, M. E. 1994, *Phys. Rev. E* 49, 3735
- Kandrup, H. E., Mahon, M. E., Smith, H. 1993, *A&A*, 271, 440
- Kandrup, H. E., Siopis, C. 2003, *MNRAS*, submitted
- Kandrup, H. E., Vass, I. M., Sideris, I. V. 2003, *MNRAS*, in press (astro-ph/0211056)
- Kormendy, J., Bender, R. 1996, *ApJ Lett.*, 464, 119
- Lauer, T. et al, 1995, *AJ*, 110, 2622
- Lauer, T. et al, 2002, *AJ*, 124, 1975
- Lichtenberg, A. J., Lieberman, M. A. 1992, *Regular and Chaotic Dynamics*, Springer, New York.
- Lynden-Bell, D. 1967, *MNRAS*, 136, 101
- Merritt, D. 2001, *ApJ*, 556, 445
- Merritt, D., Fridman, T. 1996, *ApJ*, 460, 136
- Merritt, D., Valluri, M. 1996, *ApJ*, 471, 82
- Quinn, P. J., Zurek, W. H. 1988, *ApJ*, 331, 1

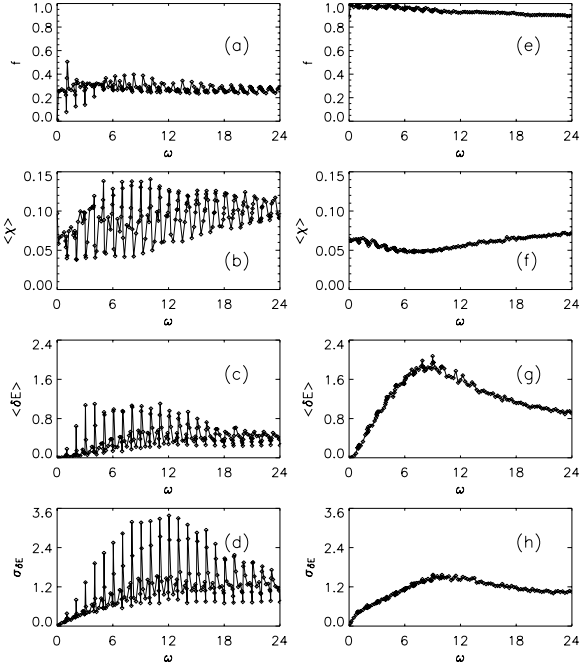


Fig. 1.— (a) The fraction f of strongly chaotic orbits in a 1600 orbit ensemble with initial energy $E = 0.87$ and mean initial radius $\langle r_{in} \rangle \approx 0.86$, evolved in a spherical oscillator potential with $M = 0.05$, $r_h = 0.3$, and $a^2 = b^2 = c^2 = 1.0$, plotted as a function of frequency ω . (b) The mean value $\langle \chi \rangle$ of the largest finite time Lyapunov exponent for the strongly chaotic orbits. (c) The mean shift in energy $\langle \delta E \rangle$ for all the orbits. (d) The dispersion $\sigma_{\delta E}$ for all the orbits. (e) - (h) The same as the preceding for orbits integrated in a potential with $a^2 = 1.33$, $b^2 = 1.0$, and $c^2 = 0.80$ and an ensemble with $E = 0.87$ and $\langle r_{in} \rangle \approx 0.89$.

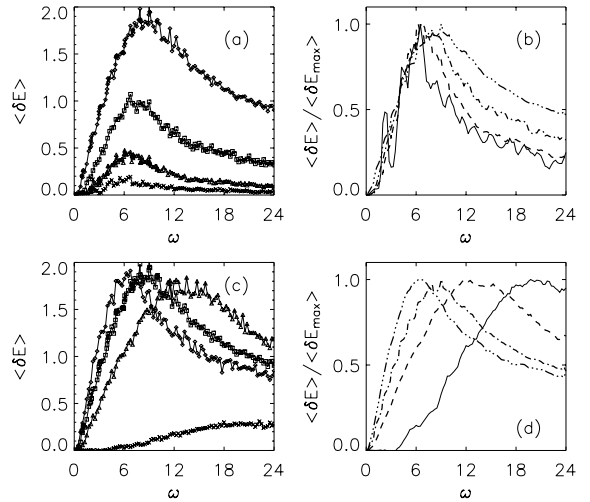


Fig. 2.— (a) The mean energy shift $\langle \delta E \rangle$ for the same ensemble used to generate FIG. 1 (e) - (h), integrated with $r_h = 0.3$, $a^2 = 1.33$, $b^2 = 1.0$, $c^2 = 0.80$, and (from top to bottom) $M = 0.05$, $M = 0.0281$, $M = 0.0158$, and $M = 0.005$. (b) $\langle \delta E \rangle$ for the same ensembles – solid line for $M = 0.005$, dashed line for $M = 0.0158$, dot-dashed line for $M = 0.0281$, and triple-dot-dashed for $M = 0.05$ – now expressed in units of the maximum shift $\langle \delta E_{max} \rangle$. (c) The mean energy shift $\langle \delta E \rangle$ for integrations with $a^2 = 1.33$, $b^2 = 1.0$, $c^2 = 0.80$, $M = 0.05$, and (curves peaking from left to right) $r_h = 0.4$, $r_h = 0.3$, $r_h = 0.2$, and $r_h = 0.1$. (d) $\langle \delta E \rangle$ expressed in units of the maximum shift $\langle \delta E_{max} \rangle$ – solid line for $r_h = 0.1$, dashed for $r_h = 0.2$, dot-dashed for $r_h = 0.3$, and triple-dot-dashed for $r_h = 0.4$.

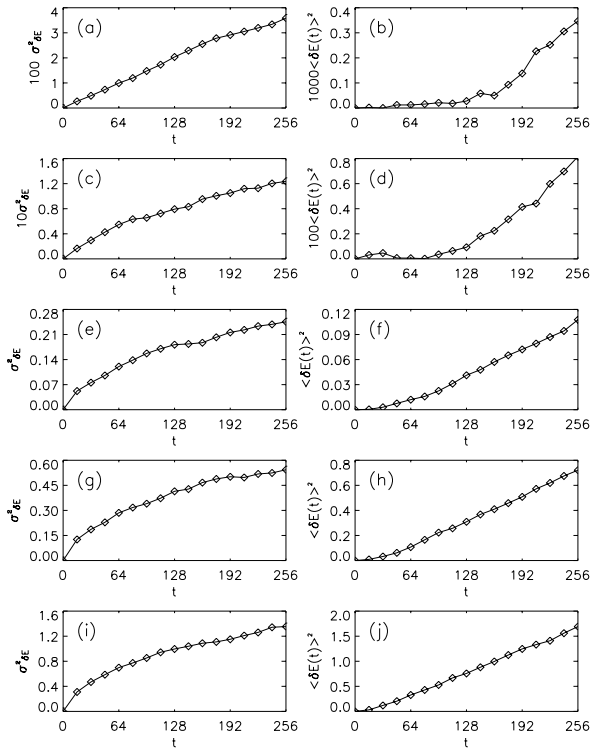


Fig. 3.— (a) $\sigma_{\delta E}^2$, where $\sigma_{\delta E}(t)$ is the time-dependent spread in energy shifts associated with an ensemble of orbits evolved in an oscillator potential with $M = 0.05$, $r_h = 0.3$, $a^2 = 1.33$, $b^2 = 1.0$, $c^2 = 0.80$ and $\omega = 0.5$. (b) $\langle \delta E(t) \rangle^2$ for the same ensemble. (c) and (d) The same for $\omega = 1.0$. (e) and (f) The same for $\omega = 2.0$. (g) and (h) The same for $\omega = 4.0$. (i) and (j) The same for $\omega = 8.0$.

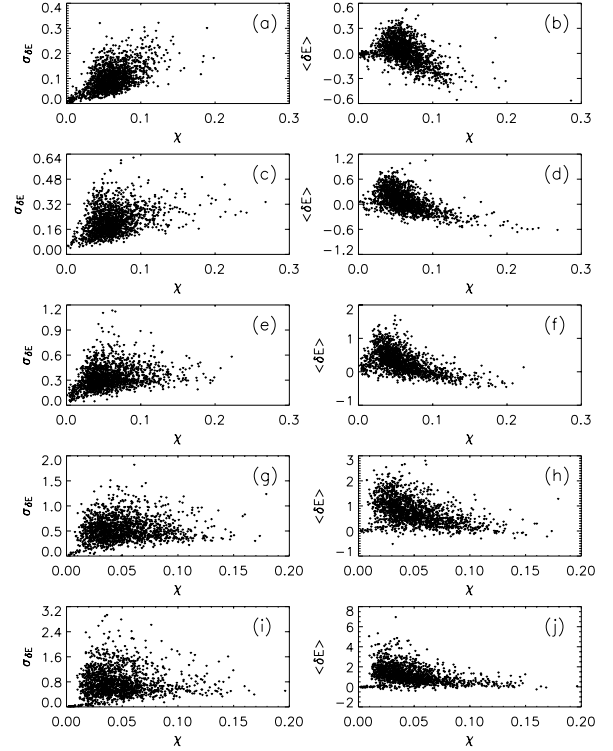


Fig. 4.— (a) Scatter plots relating $\sigma_{\delta E}$ and χ , where $\sigma_{\delta E}$ represents the dispersion associated with the time-dependent $\delta E(t)$ for an individual orbit over the interval $0 < t < 512$. The orbits are the same that were used to generate FIG. 3, integrated with $\omega = 0.5$. (b) Scatter plots relating $\langle \delta E \rangle$ and χ , where $\langle \delta E \rangle$ represents the mean value of $\delta E(t)$, computed for the same orbits as in (a). (c) and (d) The same for $\omega = 1.0$. (e) and (f) The same for $\omega = 2.0$. (g) and (h) The same for $\omega = 4.0$. (i) and (j) The same for $\omega = 8.0$.

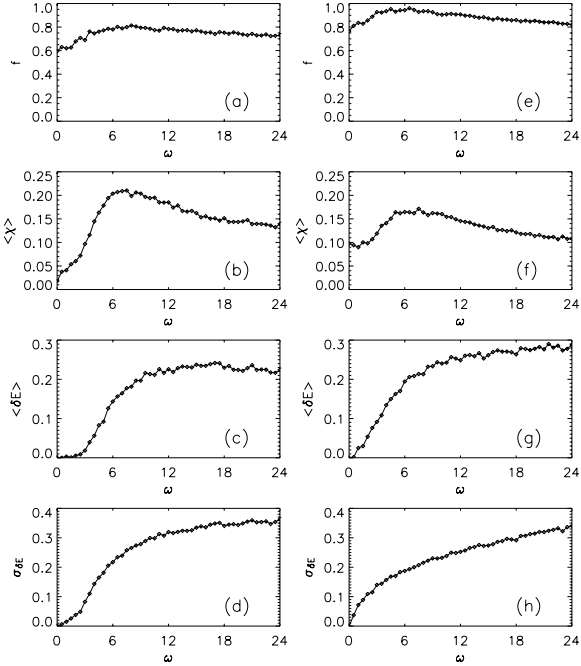


Fig. 5.— (a) The fraction f of strongly chaotic orbits in a 1600 orbit ensemble with initial energy $E = -0.70$ and mean initial radius $\langle r_{in} \rangle \approx 0.33$, evolved in a spherically symmetric Dehnen potential with $\gamma = 1.0$, $M = 0.01$, $r = 0.05$, and $a^2 = b^2 = c^2 = 1.00$. (b) The mean value $\langle \chi \rangle$ of the largest finite time Lyapunov exponent for the strongly chaotic orbits. (c) The mean shift in energy $\langle \delta E \rangle$ for all the orbits. (d) The dispersion $\sigma_{\delta E}$ for all the orbits. (e) - (h) The same as the preceding for orbits integrated in a potential with $a^2 = 1.25$, $b^2 = 1.00$, and $c^2 = 0.75$, again for an ensemble with $E = -0.70$ and $\langle r_{in} \rangle \approx 0.33$.

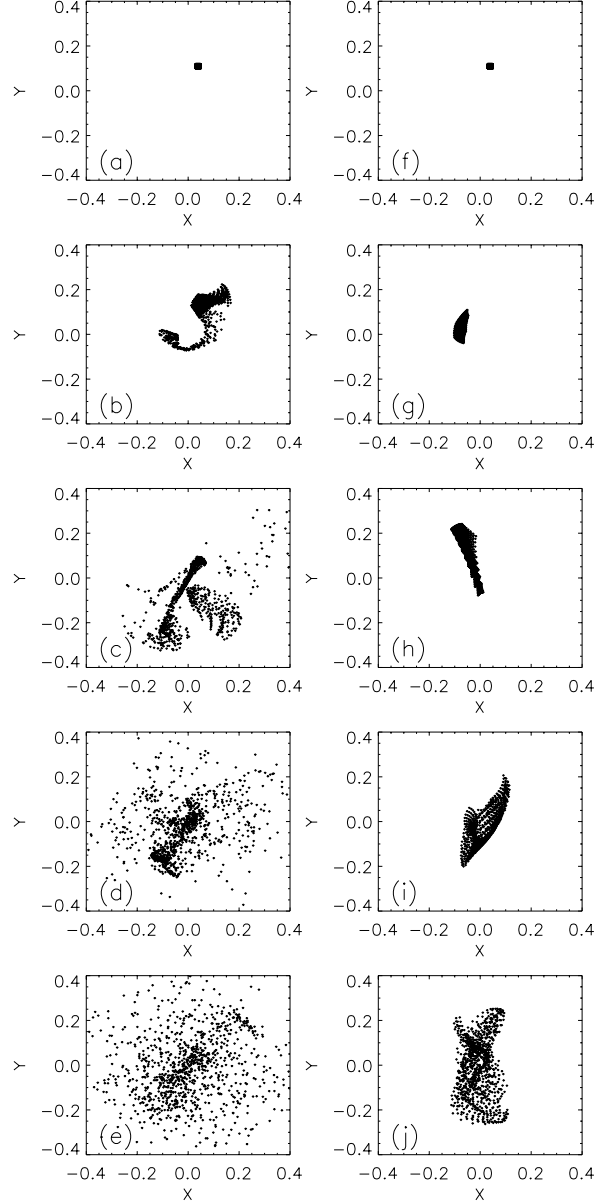


Fig. 6.— (a) The x and y coordinates at $t = 0$ for an initially localised ensemble of orbits with $E = -0.70$ and $\langle r_{in} \rangle \approx 0.33$, evolved in a spherical Dehnen potential with $\gamma = 1.0$, $r_h = 0.05$, $M = 0.005$, and $\omega = \sqrt{10}$. (b) $t = 8$. (c) $t = 16$. (d) $t = 32$. (e) $t = 64$. (f) - (j). The same for stationary black holes, *i.e.*, $\omega = 0.0$.

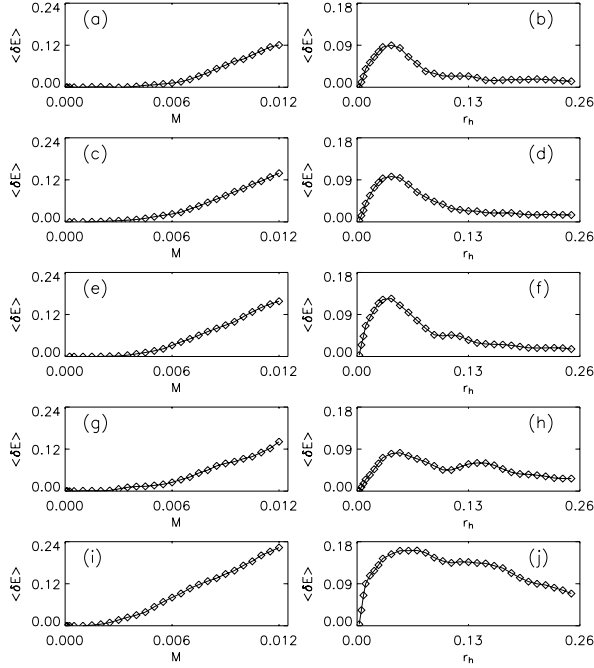


Fig. 7.— (a) The mean shift in energy, $\langle \delta E \rangle$, computed for an ensemble of orbits with $E = -0.70$ and $\langle r \rangle \approx 0.33$, evolved in a $\gamma = 1.0$ Dehnen model with $a^2 = b^2 = c^2 = 1$ in the presence of a supermassive binary comprised of two black holes executing strictly circular orbits with $r_h = 0.05$ and different values of $M_1 = M_2 \equiv M$. (b) $\langle \delta E \rangle$ for the same ensemble evolved in the same Dehnen model, again allowing for a binary executing circular orbits, but now with $M_1 = M_2 = 0.01$ and variable r_h . (c) and (d) The same for a model with $a^2 = b^2 = 0.90$ and $c^2 = 1.21$. (e) and (f) The same for a model with $a^2 = b^2 = 1.21$ and $c^2 = 0.64$ (g) and (h) The same for a model with $a^2 = 1.10$, $b^2 = 1.0$ and $c^2 = 0.90$. (i) and (j) The same for a model with $a^2 = 1.25$, $b^2 = 1.0$ and $c^2 = 0.75$. In each case, the frequency $\omega = \sqrt{(M_1 + M_2)/a^3}$, with A the semi-major axis.

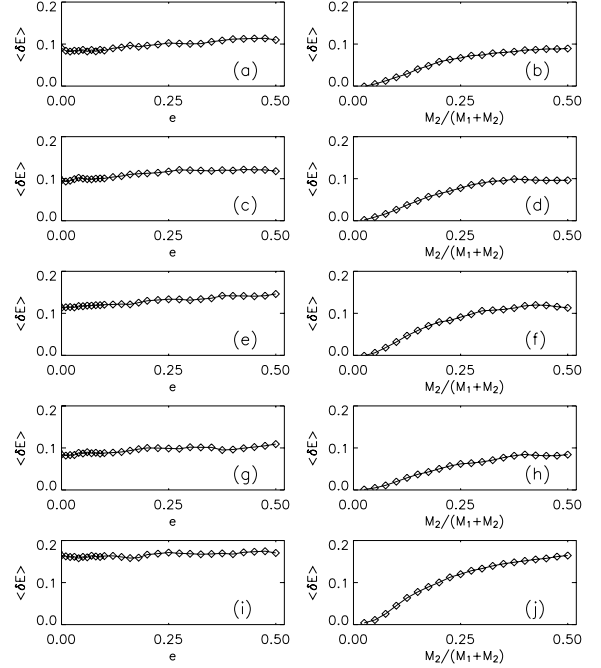


Fig. 8.— (a) The mean shift in energy, $\langle \delta E \rangle$, computed for an ensemble of orbits with $E = -0.70$ and $\langle r \rangle \approx 0.33$, evolved in a $\gamma = 1.0$ Dehnen model with $a^2 = b^2 = c^2 = 1$ in the presence of a supermassive binary comprised of two black holes with mass $M_1 = M_2 = 0.01$ executing orbits with semi-major axis $A = 0.10$ and variable eccentricity e . (b) $\langle \delta E \rangle$ for the same ensemble evolved in the same Dehnen model, again assuming $M_1 + M_2 = 0.02$ and $a = 0.10$, but now allowing for different ratios $M_2/(M_1 + M_2)$. (c) and (d) The same for a model with $a^2 = b^2 = 0.90$ and $c^2 = 1.21$. (e) and (f) The same for a model with $a^2 = b^2 = 1.21$ and $c^2 = 0.64$ (g) and (h) The same for a model with $a^2 = 1.10$, $b^2 = 1.0$ and $c^2 = 0.90$. (i) and (j) The same for a model with $a^2 = 1.25$, $b^2 = 1.0$ and $c^2 = 0.75$.

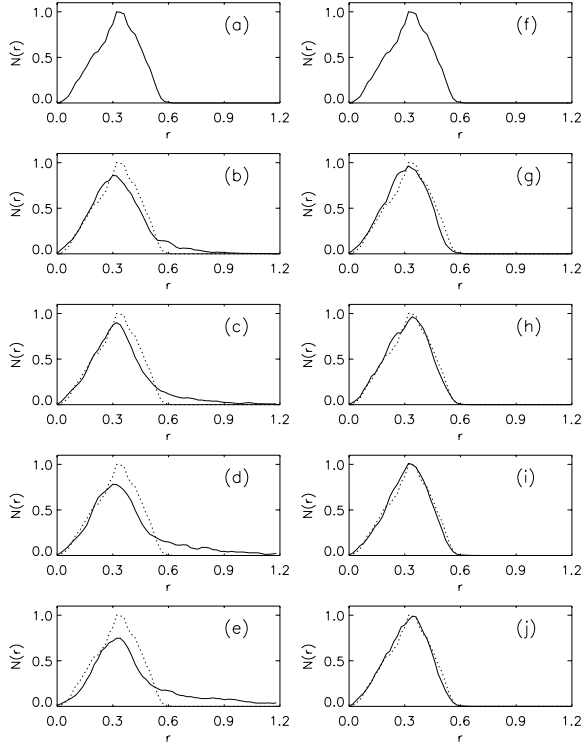


Fig. 9.— (a) The initial angle-averaged radial density distribution associated with a 4800 orbit sampling of the $E = -0.70$ constant energy hypersurface, subsequently integrated in a pseudo-Dehnen potential with $\gamma = 1.0$, $M = 0.01$, $r_h = 0.05$, $a^2 = 1.25$, $b^2 = 1.00$, $c^2 = 0.75$ and $\omega = \sqrt{20}$. (b) The density at $t = 16$. (The dotted line reproduces the initial distribution.) (c) $t = 32$. (d) $t = 64$. (e) $t = 128$. (f) - (j) The same for stationary black holes, *i.e.*, $\omega = 0.0$.

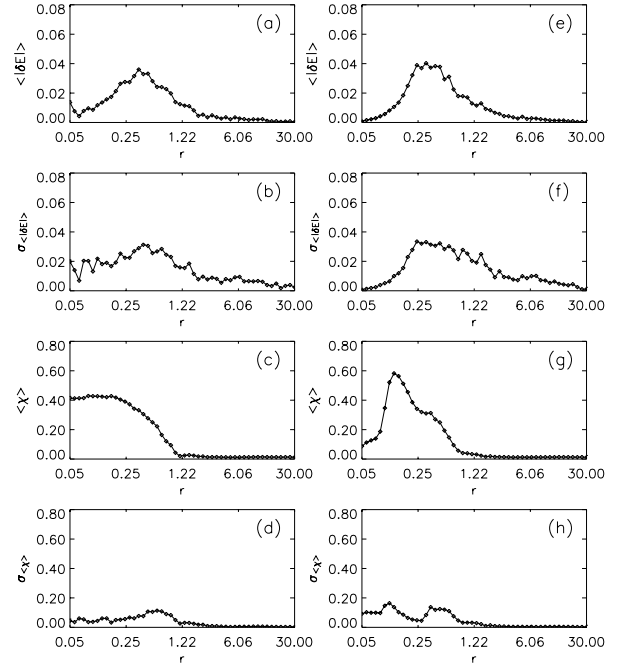


Fig. 10.— (a) Mean energy shift $\langle \delta E \rangle$, computed for ensembles with different radii, for orbits in a spherical Dehnen model with $\gamma = 0.0$ and $a = b = c = 1.0$ and black hole parameters $M = 0.005$, $r_h = 0.25$, and $\omega = 0.2828$. (b) The dispersion $\sigma_{\delta E}$ for the same ensembles. (c) The mean value $\langle \chi \rangle$ for each ensemble. (d) The dispersion σ_{χ} . (e) - (h) The same for a model with $\gamma = 1.0$.

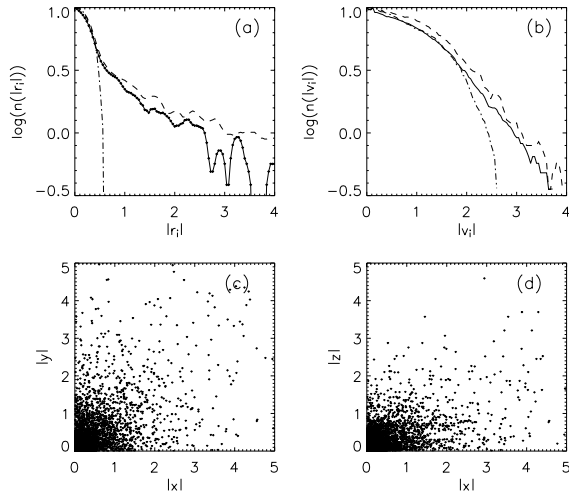


Fig. 11.— (a) The direction-dependent spatial distributions $n(|x|)$ (solid curve) and $n(|z|)$ (dashes) at $t = 512$ generated for a 4800 orbit sampling of the $E = -0.70$ hypersurface with $\gamma = 1.0$, $M = 0.01$, $r_h = 0.005$, $a = b = c = 1$, and $\omega = \sqrt{20}$, along with the distribution $n(|x|)$ (dot-dashed) at time $t = 0$. (b) The corresponding direction-dependent velocity distributions. (c) x and y coordinates for the ensemble at $t = 512$. (d) x and z coordinates for the ensemble at $t = 512$.

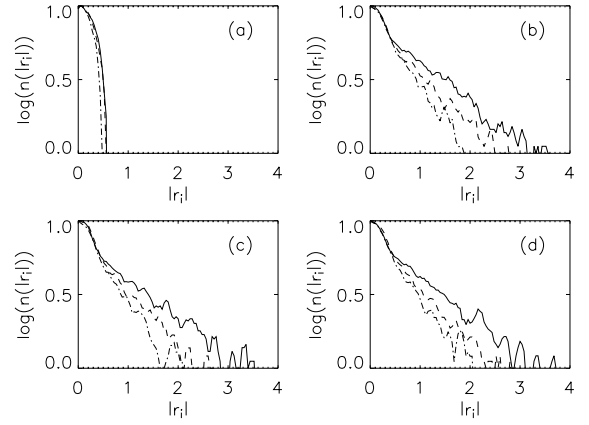


Fig. 12.— Direction-dependent spatial distributions $n(|x|)$ (solid curve), $n(|y|)$ (dashes), and $n(|z|)$ (dot-dashes) generated for a 4800 orbit sampling of the $E = -0.62$ hypersurface with $\gamma = 1.0$, $M = 0.01$, $r_h = 0.005$, $a^2 = 1.25$, $b^2 = 1.0$, $c^2 = 0.75$, and $\omega = \sqrt{20}$. along with the distribution $n(|x|)$ (dot-dashed) at time $t = 0$. (a) The distributions at time $t = 0$. (b) The distributions at $t = 512$, allowing for a binary orbiting in the $x - y$ plane. (c) The same for a binary in the $y - z$ plane. (d) The $z - x$ plane.

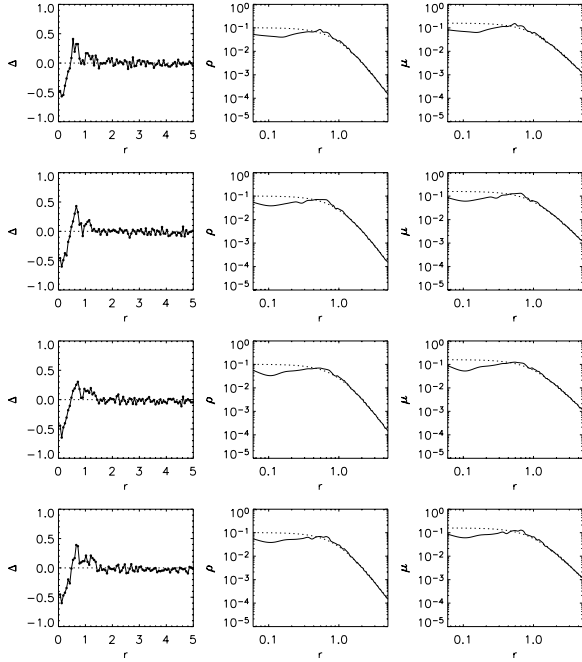


Fig. 13.— Computed quantities for a Nuker model with $\alpha = 2$, $\beta = 4$, $\gamma = 0$, $M_{BH} = 0.005$, $r_h = 0.15$, and $\omega = 0.6086$. The first column exhibits Δ , the relative fluctuation in density for different shells; the second exhibits the interpolated smooth density ρ ; the third exhibits the surface brightness, assuming that mass traces light. From top to bottom, rows represent integration times $t = 128, 256, 384$, and 512 . In each case, the dotted lines represent the original unperturbed values.

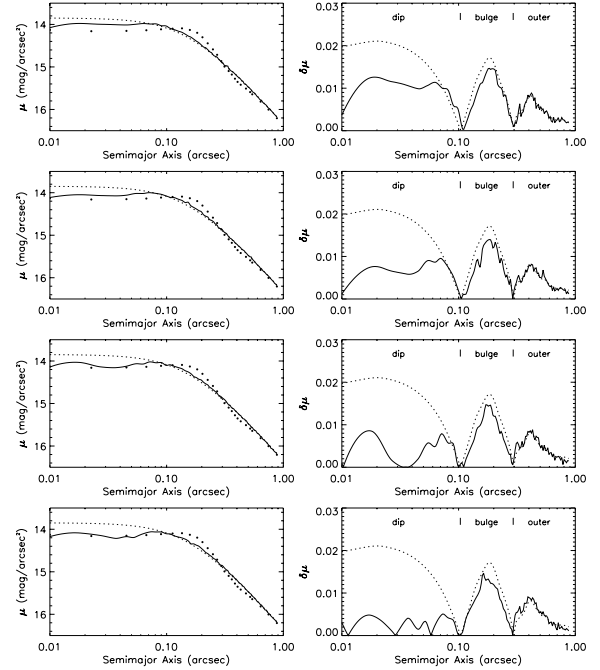


Fig. 14.— Modeling *NGC 3706* with a Nuker model with $\alpha = 2$, $\beta = 4$, $\gamma = 0$, $r_h = 0.025$, and $\omega = 8.968$. The left column exhibits the observed surface brightness profile (solid circles), the surface density predicted by an unperturbed Nuker Law (dotted lines), and the time-dependent surface density generated by the binary (solid lines) at times (from top to bottom) $t = 32, t = 64, t = 128$, and $t = 256$. The right column exhibits the relative error of the the fit for a Nuker model without (dashes) and with the binary (solid lines).

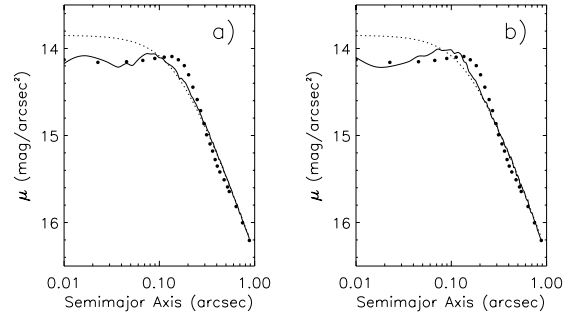


Fig. 15.— (a) The best fit model with $\alpha = 2$, $\beta = 4$, $\gamma = 0$, $r_h = 0.025$, and $\omega = 8.968$ at time $t = 256$. (b) The same, except assuming $r_h = 0.085$ and $\omega = 1.567$.